ADVANCED HEALTHCARE MATERIALS
www.advhealthmat.de

A Conformable, Gas-Permeable, and Transparent Skin-Like Micromesh Architecture for Glucose Monitoring

Ya-Lei Li, Yan-Hua Liu, Lin-Sen Chen, and Jian-Long Xu**

Monitoring the concentration of useful biomarkers via electronic skins (e-skins) is highly important for the development of wearable health management systems. While some biosensor e-skins with high flexibility, sensitivity, and stability have been developed, little attention has been paid to their long-term comfortability and optical transparency. Here, a conformable, gas permeable, and transparent skin-like Cu_2O@Ni micromesh structural glucose monitoring patch is reported. With its self-supporting micromesh structure, the skin-like glucose monitoring patch exhibits excellent shape conformability, high gas permeability, and high optical transmittance. The skin-like glucose biosensor achieves real-time monitoring of glucose concentrations with high sensitivity (15 420 μA $cm^{-2}mM^{-1}$), low detection limit (50 nM), fast response time (<2 s), high selectivity, and long-term stability. These desirable performance properties arise from the synergistic effects of the self-supporting micromesh configuration, high conductivity of the metallic Ni micromesh, and high electrocatalytic activities of the Cu_2O toward glucose. This work presents a versatile and efficient strategy for constructing conformable, gas permeable, and transparent biosensor e-skins with excellent practicability towards wearable electronics.

1. Introduction

Circulating nutrients and metabolites are useful biomarkers of biological processes in the human body, and their concentrations have been widely monitored for assessment of a human's health at a biomolecular level.[1–3] Many advances in biomedical measurements and diagnostic technologies have been achieved, and simultaneously, the rapid development of semiconductor-based devices has led to a boom in wearable devices (or wearables) that can be worn on human skin and body for continuous health metrics monitoring.[4–8] These devices give the wearers insights into the dynamics of their own physiology and allow them to actively monitor their own health.[9] The primary task is to develop various physical and chemical sensors that can be integrated into wearable formats such as wristbands, clothing, and patches to track a range of biological indicators. Among various biofluids, sweat shows great prospects for wearable sensing, because it can be generated non-invasively and on-demand. The ease of access and rich composition give sweat great potential to be adopted to evaluate the health state of individuals at a chemical and biomolecular state. Wearable sweat sensors placed close to a sweat generation site have also been developed for rapid, continuous, and non-invasive detection of a variety of sweat constituents such as chloride concentration for cystic fibrosis diagnosis, glucose concentration for diabetes management, and uric acid for cardiovascular disease diagnosis.[9–12] Yet, the development of wearable sweat sensors is still stagnating at the experimental and laboratory stage, which largely arises from the incomplete understanding of the sweat-to-blood correlation of analyte concentration. A few analytes including ethanol and chloride have been extensively investigated and correlated to the concentration in blood.[11,13–15] Preliminary correlation studies have shown promising applications for other analytes such as glucose, metabolites, and biomarkers and glucose,[16–22] including some recent works that focus on the sweat-to-blood correlation of glucose concentration in healthy individuals and subjects with diabetes.[17–22] However, more comprehensive studies should be further conducted in order to robustly establish the sweat-to-blood correlation of analyte concentration. One of the primary limitations to further push forward the large-scale tracking studies of sweat testing is how to achieve wearable sweat sensors with simultaneous measurement accuracy and wearing comfort, which can support long-term monitoring of analytes in sweat.

Since the first demonstration by Ali Javey et al., a series of sweat sensors have been developed which combined various form factors, analyte types, substrates, and detection mechanisms.[20,23–33] The sweat sensors show excellent detection performances towards various analytes and have been integrated into different form factors depending on the application case. For acquiring more accurate results, patch-style formats that can be

Y.-L. Li, Dr. Y.-H. Liu, Prof. L.-S. Chen
School of Optoelectronic Science and Engineering
Soochow University
Suzhou, Jiangsu 215006, P. R. China
E-mail: yhliu@suda.edu.cn
Dr. J.-L. Xu
Institute of Functional Nano & Soft Materials (FUNSOM)
Jiangsu Key Laboratory for Carbon-Based Functional Materials & Devices
Soochow University
Suzhou, Jiangsu 215123, P. R. China
E-mail: xujianlong@suda.edu.cn

The ORCID identification number(s) for the author(s) of this article can be found under https://doi.org/10.1002/adhm.202100046

DOI: 10.1002/adhm.202100046

conformably adhered to human skin and allow greater flexibility for their location are preferable. A critical requirement for such patch-style sensor systems is that they minimally impact the user's mobility and comfort for on-body use. For these reasons, sensors are ideally fabricated on substrates that are soft and deformable and not delaminated from the underlying skin such as paper,[9,33] polyethylene terephthalate,[11,23,20,29–33] polyimide (PI),[10,24] and nitrile[27] substrates. While high flexibility and deformability have been achieved in reported wearables with excellent detection performances using the above-mentioned substrates, the long-term comfortability and tight adhesion cannot be guaranteed due to low gas permeability during times of perspiration. Meanwhile, sensor devices that have high water vapor and gas permeability do not block the sweat and steam secreted by human skin, suppressing the potential risks of skin inflammation and bringing the wearers long-term comfortability. Moreover, tight adhesion to the skin is also essential for achieving accurate and robust analyte concentration information, while high optical transparency is instrumental for making wearable devices a visually perfect fit with the surrounding skin and pushing forward the practical applications of wearables. Therefore, a conformable sensor patch that simultaneously exhibits high optical transparency and high gas permeability would provide the best fit and highest comfort, along with long-time, non-invasive, and accurate analyte monitoring.

Here we designed an architecture to address these technological challenges in developing wearables. A self-supporting, skin-like micromesh architecture with excellent conformability, high gas permeability, and high optical transparency is proposed and fabricated, in which the glucose biorecognition element Cu_2O is electrodeposited onto a metallic micromesh to construct a glucose monitoring patch. The resulting glucose monitoring electrodes are ultralight weight (1.25 mg cm^{-2}), highly conformable (thickness ≈ 11 µm), highly optical transparent, (≈82%) and have excellent gas permeability (>2500 mm s^{-1} at 10 Pa) while also showing excellent glucose detection responses including a low detection limit (50 nM), high sensitivity (15 420 µA$cm^{-2}$$mM^{-1}$) and fast response (<2 s). Such excellent physical and electrochemical properties are attributed to the synergistic effects of the self-supporting micromesh configuration, the high conductivity of the metallic mesh, and high reactivity of Cu_2O towards glucose. Furthermore, the great selectivity, long-term stability, and reproducibility are verified in glucose detection, making the wearables presented here promising for large-scale applications in practical long-time glucose monitoring. The proposed electrode architecture herein, employing a metal oxide as the biorecognition element and self-supporting metallic micromesh film as a transducer, is an effective approach to design and fabricate conformable, gas-permeable, and transparent electrochemical biosensor patches for wearable applications.

2. Results and Discussion

The schematic diagram of our proposed Cu_2O@Ni micromesh film is shown in **Figure 1**a. The micromesh structural glucose monitoring patch is closely attached to human skin, and the glucose in sweat is converted to gluconolactone after being catalyzed by Cu_2O, leading to a measured current change versus glucose concentration. The novel Cu_2O@Ni micromesh patch was rationally fabricated by a scalable two-step process. The self-supporting Ni micromesh film was prepared using the direct laser writing and selective electrodeposition methods (Figure S1, Supporting Information, and more details are given in the Experimental Section) and then used as a transducer for glucose detection. Subsequently, Cu_2O was grown on the Ni micromesh using an electrochemical deposition method. The resulting Cu_2O@Ni micromesh film was ultrathin on the µm level and ultralight weight (≈1.25 mg cm^{-2}), and thus it could be attached to any arbitrarily shaped object, making it promising for wearable biosensor patch applications. The micromesh film was placed on a dandelion and could stand stably without deforming the dandelion (Figure 1b), confirming the extreme lightweight and excellent shape-conformable properties of the Cu_2O@Ni micromesh film. Meanwhile, the clearly visible "Campus Scenery of Soochow University" postcard beneath the micromesh film shows its high optical transparency (Figure 1c,d). From the perspective of the naked eye, the prepared glucose monitoring patch could be closely attached to a human arm or finger, indicating its excellent skin adhesion and optical transparency (Figure 1e,f). To further investigate its skin adhesion at the micron level, we used optical coherence tomography (OCT) to characterize the Cu_2O@Ni micromesh film attachment to a human arm and finger. Here, the micromesh film was transferred to the human arm and finger by the "face-to-face" water transferring method without the use of any adhesive. The face-to-face water transfer printing technology overcomes the difficulty: the micromesh patch is transferred directly and easily to the target human skin, and can be adhered to the human skin. As shown in Figures 1g,h, the Cu_2O@Ni micromesh film glucose monitoring patch was tightly adhered to human skin, confirming its excellent shape conformability, and a fine hair beneath the patch was still clearly visible. The self-supporting Cu_2O@Ni micromesh film also exhibited high optical transparency ($T \approx 82\%$) over the entire visible-band, as depicted in Figure 1i. Moreover, the gas permeability of the Cu_2O@Ni micromesh films was measured to be >2500 mm s^{-1} at an air pressure of 10 Pa (Figure 1j), which was significantly higher than cloth textiles and previously reported wearable electronic skins. Water also could directly pass through the film, further verifying its high gas permeability (inset of Figure 1j). Such excellent shape-conformability, high gas permeability, and high optical transparency make the micromesh film promising for wearable biosensor patches due to its self-supporting micromesh configuration (Figure S2, Supporting Information). As shown in the scanning electron microscopy (SEM) images, the micromesh was formed by a uniform hexagonal array over the entire region and was intrinsically interconnected at the junctions due to the pre-defined micro-groove pattern and the selective electrodeposition process. The diagonal length and line width of the micromesh film was 150 and 5 µm, respectively. It was rather remarkable that the Ni micromesh coverage was less than 5%, which resulted in the extremely low transmittance loss and high gas permeability.

The glucose recognition element Cu_2O was grown on the metallic micromesh film using a simple electrochemical deposition method to prepare a glucose monitoring patch. After Cu_2O deposition, the hexagonally arranged micromesh structure was retained (**Figure 2**a), as well as the accompanying low optical losses (≈5%) and thus the high optical transmittance of 82% at

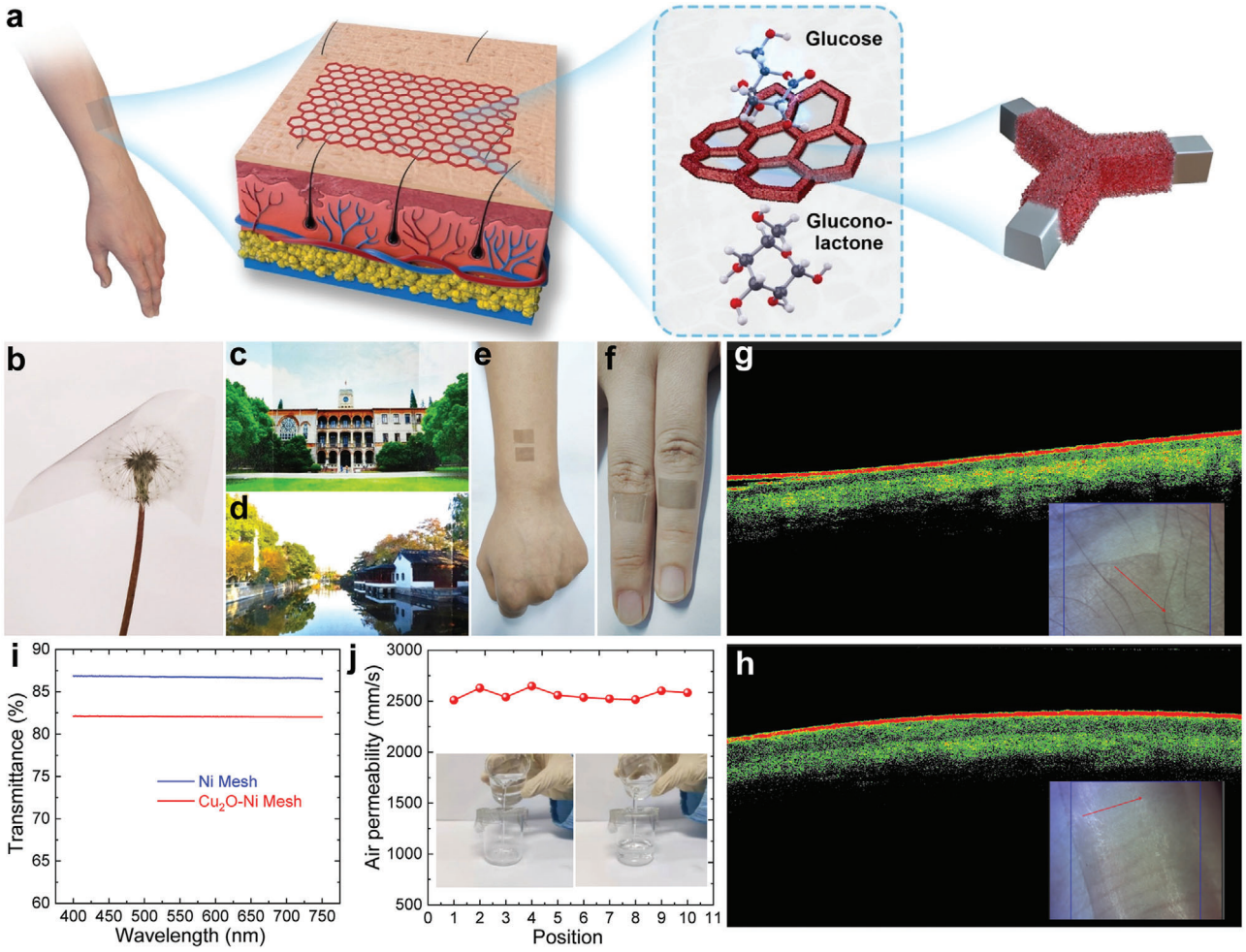

Figure 1. a) Schematic illustration of the self-supporting Cu_2O@Ni micromesh film that can be worn on human skin for continuous glucose monitoring. Digital photographs of the self-supporting Cu_2O@Ni micromesh film when placed b) on a dandelion, c,d) on a "Campus Scenery of Soochow University" postcard, and digital photographs of the self-supporting Ni and Cu_2O@Ni micromesh films e) on a human arm and f) on human fingers. OCT images of the fabricated Cu_2O@Ni micromesh film g) on a human arm, and h) on human fingers, indicating its excellent attachability and shape-conformability. The inset shows the micromesh film attached on the arm and fingers. i) Transmittance curve of the self-supporting Ni and Cu_2O@Ni micromesh films. j) The gas permeability of the self-supporting Cu_2O@Ni micromesh film under 10 Pa at different regions along the film. The inset shows that water can directly pass through the micromesh film, further supporting its high gas permeability.

550 nm (Figure 1i). Scanning electron microscopy (SEM) images (Figures 2a,b) and elemental mapping results (Figure S3, Supporting Information) demonstrated that the conformal deposition of Cu_2O, which was confirmed to be Cu_2O as discussed below, was uniformly achieved on the Ni micromesh. A dense and crack-free Cu_2O nano film composed of 100–300 nm of Cu_2O nanoparticles was wrapped around the Ni mesh (Figure 2c), forming a core-shell structure with the Ni mesh as the conductive "core" and the uniformly deposited Cu_2O layer as the active "shell" (Figure 2d). The thicknesses of Ni "core" and Cu_2O "shell" were measured to be 7.6 and 1.7 μm, respectively. Moreover, as shown in Figure 2e, in addition to the (111), (200), and (220) peaks in the X-ray diffraction (XRD) data that correspond to the Ni metal, five characteristic peaks located at 73.5°, 61.5°, 42.3°, 36.5°, 36.5°, and 29.5° that correspond to the (311), (220), (200), (111), and (110) planes in the Cu_2O phase were also observed (JCPDS nos. 78-2076),[34,35] suggesting that Cu_2O was successfully prepared on the Ni micromesh. Moreover, the Cu 2p X-ray photoelectron spectroscopy (XPS) spectrum exhibited the core-level Cu 2p1/2 and Cu 2p3/2 (Figure 2f), located at 952.2 and 932.4 eV, respectively, which was in good agreement with previous reports for Cu_2O.[35–37] The two broad peaks at 955.1 and 935.3 eV were designated as Cu 2p1/2 and Cu 2p3/2 of Cu^{2+}, respectively, suggesting the formation of amorphous CuO on the surface due to surface oxidation.

The electrocatalytic oxidation performance of the Cu_2O@Ni micromesh film was first assessed by current versus voltage (CV) measurements utilizing a standard three-electrode configuration (the experimental setup was shown in Figure S4, Supporting Information, and the micromesh film, Ag/AgCl electrode, and Pt wire was used as working electrode, counter electrode, and reference electrode, respectively), and the bare Ni micromesh film was also characterized as a comparison. **Figure 3**a presents the electrochemical performances of the bare Ni and Cu_2O@Ni

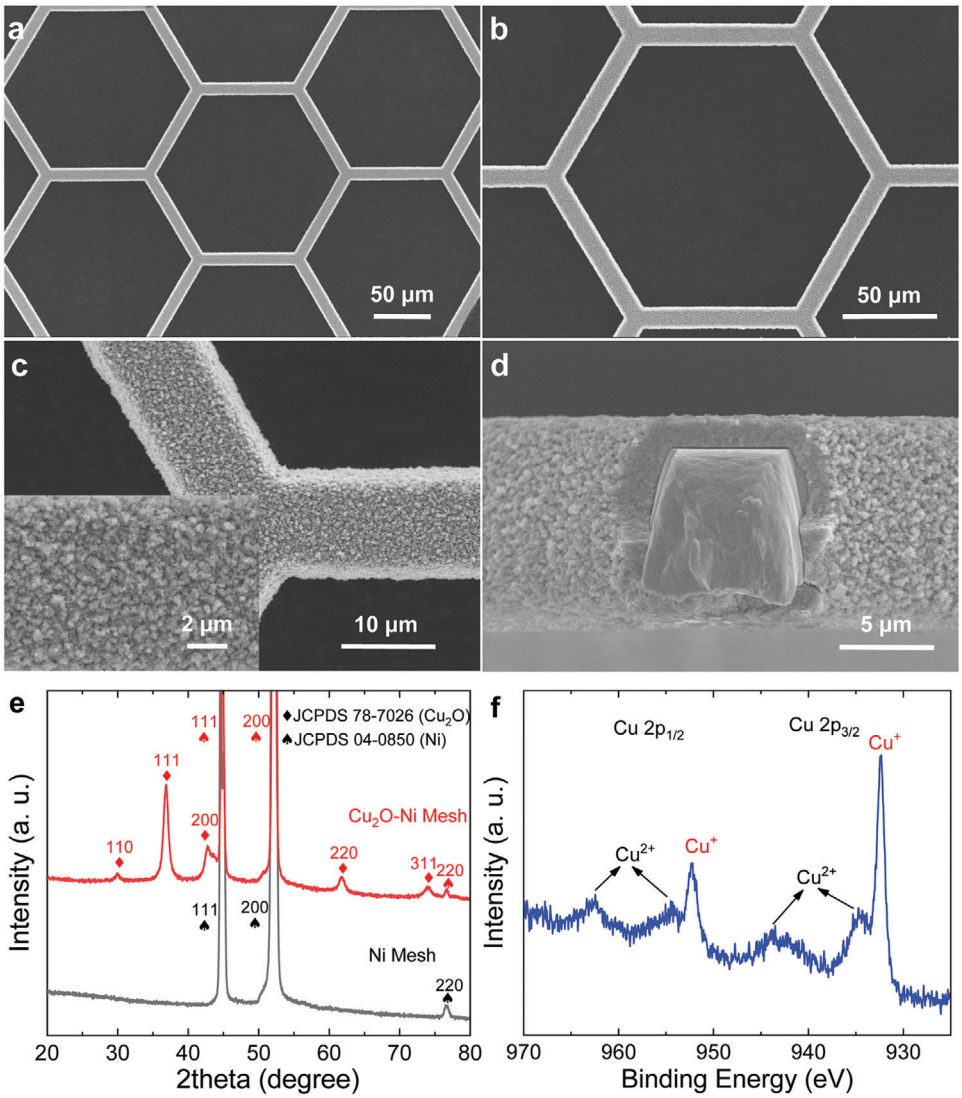

Figure 2. a,b) SEM images of the fabricated self-supporting Cu_2O@Ni micromesh film. c) SEM image of the fabricated Cu_2O@Ni micromesh film. Inset diagram reveals the high-resolution SEM image of Cu_2O nano film deposited on the Ni strings. d) Cross-sectional SEM image of the fabricated Cu_2O@Ni micromesh film showing its core-shell structure with a conductive Ni "core" and electrodeposited Cu_2O active "shell". e) XRD patterns of the self-supporting Ni micromesh film before and after the electrodeposition of glucose recognition element Cu_2O. f) XPS spectrum of Cu_2O electrodeposited on the Ni micromesh.

micromesh films in the presence and absence of 0.1 mM glucose in 0.1 M NaOH. Typical redox peak signals were seen for the Ni micromesh film in 0.1 M NaOH; however, an inappreciable current change could be observed upon glucose addition, indicating that the bare Ni micromesh film was inactive for glucose oxidation. In contrast, a remarkable cathodic current enhancement was seen in the presence of 0.1 mM glucose with the accompanied decrease of anodic peak current, suggesting the highly sensitive catalytic activity of the Cu_2O@Ni micromesh films towards glucose oxidation. Here, Cu^{3+} played a critical role in the electrocatalytic cycling reaction of Cu_2O toward glucose, as illustrated in Equations S1–S4, Supporting Information.[38] The Cu^+ on Cu_2O was firstly electrochemically oxidized to $Cu(OH)_2$ and then transformed to CuO. Then, the Cu^{2+} was electro-oxidized to Cu^{3+} (CuOOH), which catalyzed the glucose oxidation into gluconolactone, and was finally reduced to Cu(II).[38] During the electrooxidation of Cu^+, the generated electrons shuttled through the Ni micromesh into the electrochemical loops, and thus excited the current response upon glucose addition. The electrochemical kinetics of the Cu_2O@Ni micromesh film were further explored by measuring the CVs at ranging scan rates from 10 to 200 mV s^{-1} in a 0.1 M NaOH solution with 0.1 mM glucose, as illustrated in Figure 3b. It is worth noting that the current response, that is, both cathodic and anodic current densities, were enhanced with an increase in scan rate and were accompanied by a negative shift in the anodic peak potential. These responses imply a quasi-reversible electron transfer process in the glucose oxidation reaction by Cu_2O. Figure 3c depicts the linear relationship between the peak current densities and the square root of the scan rate, demonstrating a typical diffusion-controlled electrochemical

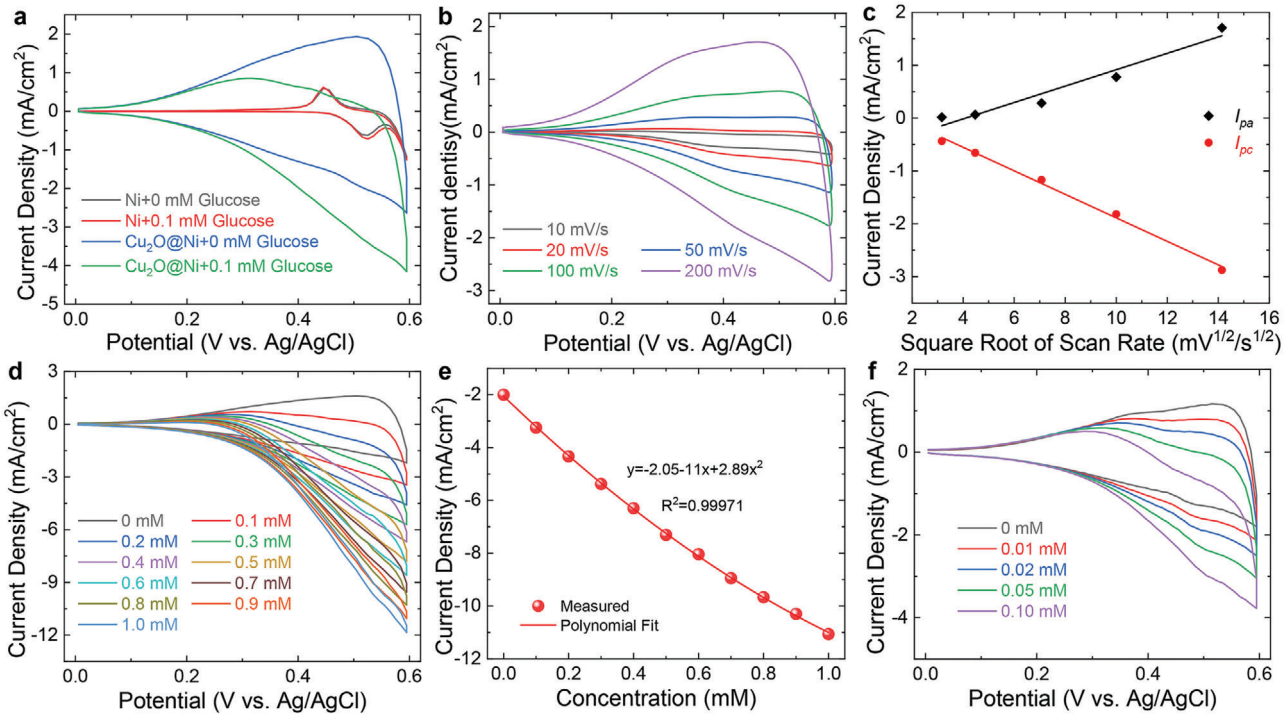

Figure 3. a) CV curves of the prepared Ni and Cu_2O@Ni micromesh films in the presence and absence of glucose (0.1 mM) in a NaOH solution (0.1 M) at 100 mV s^{-1}. b) CV curves of the Cu_2O@Ni micromesh film in a NaOH solution (0.1 M) containing glucose (0.1 mM) at different scan rates from 10 to 200 mV s^{-1}. c)The linear calibration plot of the peak current densities versus square root of scan rate extracted from Figure 3 (b). d) CV curves of the Cu_2O@Ni micromesh film at a scan rate of 100 mV s^{-1} in a NaOH (0.1 M) solution containing different concentrations of glucose (ranging from 0 to 1 mM). e) The corresponding calibration plot of panel (d). f) CV curves of the Cu_2O@Ni micromesh film in 0.1 M NaOH containing low concentrations of glucose ranging from 0 to 100 µM.

process for the redox reactions on the Cu_2O@Ni micromesh film. Moreover, to prove the feasibility of glucose monitoring using the Cu_2O@Ni micromesh film, the electrocatalytic performance was further studied in glucose concentrations ranging from 0 to 1 mM by measuring the CV curves at a scan rate of 100 mV s^{-1} (Figure 3d). Upon an increase in glucose concentrations from 0 to 1 mM with a step of 0.1 mM, the cathodic current gradually increased, whereas the anodic peak current obviously decreased. The corresponding calibration curve showed a polynomial behavior ($R^2 = 0.99971$) with the glucose concentration increasing from 0 to 1 mM. Furthermore, the Cu_2O@Ni micromesh film still exhibited an obvious current response to 10 µM glucose (Figure 3f), which further showed its great promise in practical applications and will be discussed below.

To obtain the optimal glucose sensing performance of the Cu_2O@Ni micromesh films, a range of fabrication and characterization conditions such as the Cu_2O electrodeposition time, applied potential, etc., were optimized prior to applications in glucose sensing. The optimization processes were conducted by measuring the current values at a constant applied potential with the stepwise addition of 0.1 mM glucose under constant stirring. As illustrated in Figure S5a, Supporting Information, the current response increased with an increase of Cu_2O electrodeposition time and saturated with an electrodeposition time of 600 s at a growth current density of 1 mA cm^{-2}, which was adopted for further sample preparation. The applied potential was also a vital parameter in the amperometric determination of glucose. Figure S5b, Supporting Information, exhibits the amperometric response curveunder different applied potentials of the Cu_2O@Ni micromesh film upon stepwise glucose addition. The highest response sensitivity toward glucose was achieved at 0.6 V by changing the applied potential from 0.5 to 0.65 V. Further potential increases led to a significant increase in the background noise, and thus greatly decreased the signal-to-noise ratio. Therefore, in order to achieve the best glucose-sensing performances, the glucose recognition element Cu_2O was electrodeposited on the Ni micromesh film at a current density of 1 mA cm^{-2} for 600 s, and the applied potential for glucose determination was set as 0.6 V.

The typical amperometric response curve of the Cu_2O@Ni micromesh film upon stepwise glucose addition at 0.6 V versus Ag/AgCl is shown in **Figure 4**a, and the response curve to low glucose concentrations is magnified in the inset. A steep and stable amperometric response upon the stepwise glucose addition was obtained with a fast response time (<2 s), and the current increased stepwise with successive glucose additions. This response was relatively rapid for an electrochemical glucose sensor. Moreover, the remarkable amperometric feedback was well distinguished even when the glucose concentration was as low as 50 nM, showing the high sensitivity of our fabricated Cu_2O@Ni micromesh film towards glucose oxidation. The corresponding calibration curve extracted from the amperometric response results is plotted in Figure 4b, which could be broken into two linear regions with a high sensitivity of 15 420 µAcm^{-2} mM^{-1} at low concentrations from 50 nM to 118.25 µM and high

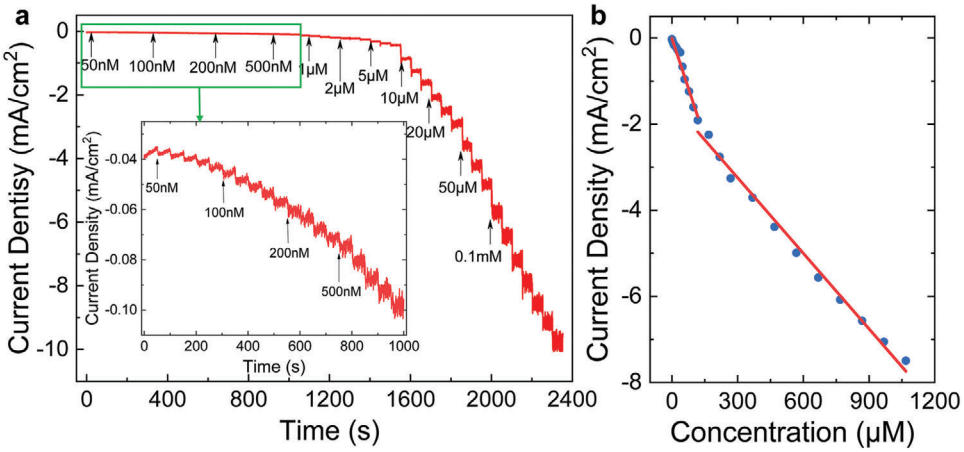

Figure 4. a) Typical amperometric response to stepwise glucose addition in 0.1 M NaOH at a constant applied potential of 0.6 V (versus Ag/AgCl). Inset shows the response curve to low glucose concentrations ranging from 50 to 500 nM. b) The corresponding calibration plot of current density versus glucose concentration extracted from panel (a).

Table 1. Comparison of the glucose detection performances and physics characteristics of the proposed Cu_2O@Ni micromesh film in this work with other previously reported glucose-sensing elements.

Electrodes	Transparent	Flexible	Response time [s]	Sensitivity [μAcm^{-2} mM^{-1}]	LDL [μM]	Reference
CuO@C/D	No	No	<3	1650	0.5	[39]
ISFETs	Yes	Yes	-	18–45	-	[40]
Ni-Cu/PGE	No	No	2	2951	0.99	[41]
Cu NWs	No	No	-	420.3	0.035	[42]
α-IGZO FET	Yes	No	-	-	170	[43]
CuO/CFF	No	Yes	1.3	6476	0.27	[44]
Cu_2O SLNs	No	No	≈3	933	0.035	[45]
NiO-BP2	No	Yes	<2.5	2701	14	[46]
CuO/MWCNTs	No	No	≈1	2596	0.2	[47]
Cu_2O@Ni mesh	Yes	Yes	<2	15 420	0.05	This work

Abbreviations: LDL, lowest detection limit; CuO@C/D, CuO@carbon nanowalls/diamond; ISFETs, ion-sensitive field-effect transistors; PGE, pencil graphite electrode; α-IGZO FET, amorphous InGaZnO field-effect transistor; CFF, carbon fiber fabric; SLNs, shuriken-like nanostructures; MWCNTs, multi-walled carbon nanotubes.

sensitivity of 5850 μAcm^{-2} mM^{-1} from 118.25 μM to 1.07 mM. In addition, the glucose-sensing performance, as well as the physical properties of the Cu2O@Ni micromesh film, are summarized and compared with previous reported non-enzymatic glucose biosensors,[39–47] as shown in **Table 1**. It can be clearly seen that our proposed Cu_2O@Ni micromesh film exhibited higher sensitivity than most of the reported glucose biosensors, and more impressively, this sensitivity was achieved while also achieving excellent shape conformability, high gas permeability, and high optical transparency. Moreover, the response time and lowest detection concentration were also superior or comparable to most reported glucose biosensors. The proposed Cu_2O@Ni micromesh film had excellent adhesion between the Ni micromesh and Cu_2O due to the use of chemical electrodeposition methods. Together with the scalability of Ni micromesh creation with industrially-relevant techniques including direct laser writing and selective electrodeposition, these micromesh films exhibit superior reproducibility and feasibility for large-scale and array production, and hold great potential in practical determination of glucose levels.

The accuracy of glucose detection in the presence of other biomarkers is critical for practical applications of non-enzymatic electrochemical glucose biosensors. As reported in previous literatures, except for glucose, many interferents including Na^+ (10–100 mM in sweat), Cl^- (10–100 mM in sweat), NH_4^+ (0.1–1 mM in sweat), ethanol (2.5–22.5 mM in sweat) and ascorbic acid (AA, 10–50 μM in sweat) are simultaneously existed in sweat[9] (note that the maximum concentration of glucose and the main interferents is adopted for selectivity characterizations), and they may produce comparable oxidation currents in the sensor and could interfere with its response toward glucose. Here, the selectivity performances of the proposed Cu_2O@Ni micromesh film were also evaluated by recording the amperometric current response with the successive addition of 0.2 mM glucose, 100 mM NaCl, 1 mM NH_4Cl, 22.5 mM ethanol, and 50 μM AA. As shown in **Figures 5**a,b, these interferents had a negligible effect on the glucose response; typically, the ratios of the response to the interferents compared to the glucose signals were all less than 6%, verifying excellent selectivity performances of our proposed Cu_2O@Ni micromesh electrode when adopted for practical glucose

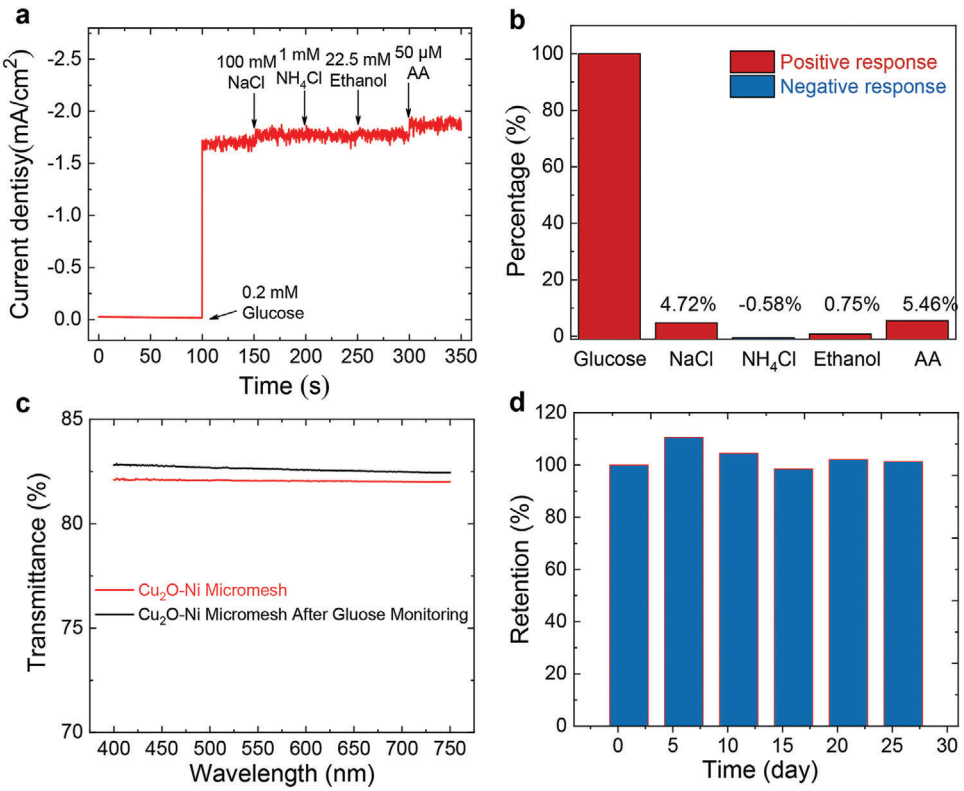

Figure 5. a) Amperometric response of the self-supporting Cu_2O@Ni micromesh film toward the successive addition of 0.2 mM glucose, 100 mM NaCl, 1 mM NH_4Cl, 22.5 mM ethanol, and 50 μM AA in 0.1 M NaOH. b) Ratio of the interfering noise to the glucose-sensing signal extracted from panel (a). c) Transmittance spectra of the Cu_2O@Ni micromesh film before and after 1800 s of continuous glucose monitoring. d) Long-term air and light stability properties of the Cu_2O@Ni micromesh film for glucose detection in 0.1 M NaOH every 6 days over 26 days. Here, the micromesh film is stored in air ambient and under indoor light illumination without any encapsulation.

concentration detection in sweat. Moreover, the long-term stability of the fabricated micromesh film was estimated from the aspects of optical transparency and glucose sensing performances. Figure 5c shows the transmittance spectra of the Cu_2O@Ni micromesh film before and after successive glucose addition for 1800 s. The optical transmittance varied little after 1800 s of continuous glucose monitoring, and the little transmittance variation possibly arose from the Cu_2O morphology change after glucose oxidation (shown in Figure S6, Supporting Information) and some measurement errors. The glucose sensing performance stability was estimated by measuring the current responses toward 0.1 mM glucose using the CV method every 6 days with storing in air ambient and under indoor light illumination without any encapsulation and light protection over successive 26 days. The CV measurements were conducted from 0 to 0.6 V at a scan rate of 100 mV s^{-1} in 0.1 M NaOH with 0.1 mM glucose. The current response retained almost 100% of its initial value after storing the sensor in air ambient for 26 days (Figure 5d), indicating the excellent air stability of the Cu_2O@Ni micromesh film. In addition, three parallel micromesh films were prepared using the same fabrication methods and were used to determine the glucose levels. All three micromesh films exhibited almost consistent glucose-sensing performances and air stability properties (Figure S7, Supporting Information), suggesting great reproducibility of our proposed Cu_2O@Ni micromesh film as a high-performance wearable glucose monitoring patch.

As discussed above, in addition to its excellent shape conformability, high gas permeability, and high optical transparency, the proposed Cu_2O@Ni micromesh film also exhibited excellent glucose-sensing performances including low detection limit, high sensitivity, fast response time, great selectivity, excellent long-term stability, and high reproducibility. It can be ascribed from several synergistic effects in the designed architecture. 1) The micromesh structure facilitated efficient electrolyte penetration and diffusion into the Cu_2O, meaning thicker Cu_2O up to μm in scale (≈1.7 μm in our micromesh film), can be deposited and still show effective and efficient glucose oxidation. Thus, this micromesh structure simultaneously leads to high optical transparency and high glucose catalytic activities. 2) The core-shell structure with the conductive Ni micromesh as the "core" and the glucose recognition Cu_2O as the "shell" induced synergistic interactions between the Ni mesh and Cu_2O, where the highly conductive Ni micromesh worked as great current collector and the Cu_2O was wrapped around the Ni micromesh. This core-shell structure yielded enhanced conductivity and catalytic activities, which facilitated the electron transport in the electrocatalytic reactions. 3) The direct and strong binding of the Cu_2O to the conductive Ni micromesh without adding extra polymer binders

ensured high mass-transport kinetics as well as eliminated partial blocking of the electroactive regions. 4) The core-shell Cu_2O@Ni micromesh structure possessed excellent structural and mechanical stability, which led to long-term cycling stability for glucose determination.

3. Conclusion

In summary, a novel, self-supporting, skin-like micromesh architecture was rationally designed to achieve a conformable, gas permeable, and transparent glucose monitoring patch for wearable applications. The Ni micromesh film was fabricated by direct laser writing and selective electrodeposition, followed by electrodeposition of the glucose recognition element, Cu_2O. The well-designed Cu_2O@Ni micromesh film was ultralight weight (1.25 mg cm^{-2}, including Ni and Cu_2O), highly shape conformable (thickness ≈ 11 µm), highly optical transparent (≈82%), and had excellent gas permeability (>2500 mm s^{-1} at 10 Pa), while also showing excellent performance as a glucose sensor including a low detection limit (50 nM), high sensitivity (15 420 µAcm^{-2} mM^{-1}), and fast response (<2 s). Furthermore, remarkable selectivity, good air and light stability, and high reproducibility were also achieved in glucose detection. The above results highlight the promising potential of the Cu_2O@Ni micromesh for practical applications as a self-supporting glucose monitoring patch. More significantly, the present work presents a versatile and effective method, in which a self-supporting metallic micromesh film acts as a nanostructural and conductive transducer, to design and fabricate conformable, gas permeable, and optically transparent electrochemical biosensor patches for wearable applications.

4. Experimental Section

Materials: All chemical reagents were used as received without further purification unless stated elsewhere. D-Glucose, NaOH, and NaCl were purchased from Macklin Biochemical Co., Ltd. Lactic acid, NH_4Cl, ethanol, and Ascorbic acid (AA) were obtained from Aladdin Reagents. Copper (II) sulfate pentahydrate ($CuSO_4 \cdot 5H_2O$) was obtained from Alfa Aesar. Deionized (DI) water from Millipore ($R \geq 18.2$ MΩ cm) was used for all experiments.

Fabrication of the Self-Supporting Metallic Micromesh Film: The fabrication process of the self-supporting metallic micromesh film is illustrated as follows (Figure S1, Supporting Information): First, the photoresist (PR) layer was spin-coated onto a pre-cleaned indium tin oxide (ITO)-glass substrate, and the hexagonally -arranged groove micro-patterns were generated by the direct laser writing method. Afterward, Ni metal was selectively electrodeposited onto the patterned grooves and formed a uniform metallic micromesh film. Finally, the Ni micromesh film was easily peeled off from the ITO glass substrate after removal of the residual PR with a concentrated NaOH solution. The typical Ni micromesh film thickness was approximately 3–10 µm and could be controlled by adjusting the PR layer thickness, Ni electrodeposition current density, and Ni electrodeposition time.

Electrodeposition of Glucose Recognition Element Cu_2O: The glucose recognition element Cu_2O was electrodeposited onto the self-supporting Ni micromesh film using a standard three-electrode configuration, consisting of the Ni micromesh film as the working electrode, a platinum wire as the counter electrode, and a saturated calomel electrode as the reference electrode at room temperature. The electrolyte solution was a mixture of a 0.3 M $CuSO_4 \cdot 5H_2O$ aqueous solution and a lactic acid solution (volume ratio ≈ 3:1), and the pH of the electrolyte solution was adjusted to ≈12 by adding 5 M NaOH aqueous solution. Cu_2O was electrodeposited at a constant current density of 1 mA cm^{-2} for 600 s. The obtained Cu_2O@Ni micromesh film was thoroughly washed with DI water several times and dried at ambient conditions.

Characterization Methods: The optical transmission spectra of the micromesh films were measured using a UV–vis-spectrophotometer (SPECORD210 PLUS, Analytikjena). OCT (Telesto, THORLABS) was used to investigate the attachability of the glucose monitoring patch onto human skin. The gas permeability of the micromesh film was characterized by a textile air permeability tester (YG461E). The microstructures of Ni and Cu_2O@Ni micromesh films were studied by FE-SEM (SU8010, Hitachi Ltd.). The crystalline structure and chemical composition of the glucose recognition element Cu_2O were examined with XRD (PANalytical Empyrean, Cu *kα* radiation) and XPS with monochromatized Al *kα* radiation, respectively.

Electrochemical Tests: The glucose detection performance measurements were all performed on a CHI 760B electrochemical workstation (CH Instruments Inc., Shanghai) using a three-electrode configuration at room temperature. The self-supporting Cu_2O@Ni micromesh film was used as the working electrode, and the Ag/AgCl electrode and Pt wire served as the reference and counter electrode, respectively. Electrochemical measurements were conducted in a 0.1 M NaOH aqueous solution. All the chronoamperometric measurements were performed by applying an optimized potential to the working electrode and allowing the transient background current to decay to a steady-state value before the addition of glucose. The electrode area refers to the whole area of the micromesh film including the Ni metal area and unoccupied area for all presented measurements and calculations.

Supporting Information

Supporting Information is available from the Wiley Online Library or from the author.

Acknowledgements

All the experiments on human skin were performed under the permission by Ethics Committee of Soochow University. The volunteer in this study gave their informed, written consent, prior to the skin adhesion experiment. The authors acknowledge financial support from the National Natural Science Foundation of China (Nos. 61974100 and 61705152), the Natural Science Foundation of Jiangsu Province (No. BK20181166), the Open Foundation of State Key Laboratory of Electronic Thin Films and Integrated Devices (No. KFJJ202002) and the National Science Foundation of the Jiangsu Higher Education Institutions of China (No. 20KJA480002). This project is also funded by the Collaborative Innovation Center of Suzhou Nano Science and Technology, Key Lab of Modern Optical Technologies of Education Ministry of China, Key Lab of Advanced Optical Manufacturing Technologies of Jiangsu Province, and the "111" Project. The authors are grateful to Mr. Fei Hu for his help of graphic diagrams.

Conflict of Interest

The authors declare no conflict of interest.

Data Availability Statement

The data that support the findings of this study are available from the corresponding author upon reasonable request.

Keywords

conformable materials, gas permeable materials, glucose monitoring, micromesh architectures, optically transparent materials, wearable electronics

Received: January 9, 2021
Revised: May 24, 2021
Published online:

[1] T. J. Wang, M. G. Larson, R. S. Vasan, S. Cheng, E. P. Rhee, E. McCabe, G. D. Lewis, C. S. Fox, P. F. Jacques, C. Fernandez, C. J. O'Donnell, S. A. Carr, V. K. Mootha, J. C. Florez, A. Souza, O. Melander, C. B. Clish, R. E. Gerszten, *Nat. Med.* **2011**, *17*, 448.
[2] K. Suhre, S. Shin, A. Petersen, R. P. Mohney, D. Meredith, B. Wagele, E. Altmaier, C. Panos Deloukas, J. Erdmann, E. Grundberg, M. Mangino, C. Meisinger, T. Meitinger, H. Mewes, M. V. Milburn, C. Prehn, J. Raffler, J. S. Ried, W. Romisch-Margl, N. J. Samani, K. S. Small, H. Wichmann, G. J. Zhai, T. Illig, T. D. Spector, J. Adamski, N. Soranzo, C. Gieger, *Nature* **2011**, *477*, 54.
[3] T. Illig, C. Gieger, G. J. Zhai, W. Romisch-Margl, R. Wang-Sattler, C. Prehn, E. Altmaier, G. Lastenmuller, B. S. Kato, H. Mewes, T. Meitinger, M. Angelis, F. Kronenberg, N. Soranzo, H. Wichmann, T. D. Spector, J. Adamski, K. Suhre, *Nat. Genet.* **2010**, *42*, 137.
[4] T. Yokota, T. Nakamura, H. Kato, M. Mochizuki, M. Tada, M. Uchida, S. Lee, M. Koizumi, W. Yukita, A. Takimoto, T. Someya, *Nat. Electron.* **2020**, *3*, 113.
[5] Y. H. Liu, M. Pharr, G. A Salvatore, *ACS Nano* **2017**, *11*, 9614.
[6] K. Lee, X. Y. Ni, J. Y. Lee, H. Arafa, D. J. Pe, S. Xu, R. Avila, M. Iroe, J. H. Lee, R. L. Easterlin, D. H. Kim, H. U. Chung, O. O. Olabisi, S. Getaneh, E. Chung, M. Hill, J. Bell, H. Jang, C. Liu, J. B. Park, J. Kim, S. B. Kim, S. Mehta, M. Pharr, A. Tzavelis, J. T. Reeder, I. Huang, Y. Deng, Z. Q. Xie, C. R. Davies, Y. G. Huang, J. A Rogers, *Nat. Biomed. Eng.* **2020**, *4*, 148.
[7] J. H. Koo, S. Jeong, H. J. Shim, D. Son, J. Kim, D. C. Kim, S. Choi, J. Hong, D. H. Kim, *ACS Nano* **2017**, *11*, 10032.
[8] A. Miyamoto, S. Lee, N. F. Cooray, S. Lee, M. Mori, N. Matsuhisa, H. Jin, L. Yoda, T. Yokota, A. Itoch, M. Sekino, H. Kawasaki, T. Ebihara, M. Amagai, T. Someya, *Nat. Nanotechnol.* **2017**, *12*, 907.
[9] M. Bariya, H. Y. Y. Nyein, A. Javey, *Nat. Electron.* **2018**, *1*, 160.
[10] H. Lee, T. K. Choi, Y. B. Lee, H. R. Cho, R. Ghaffari, L. Wang, H. J. Choi, T. D. Chung, N. S. Lu, T. Hyeon, S. H. Choi, D. H. Kim, *Nat. Nanotechnol.* **2016**, *11*, 566.
[11] S. Emaminejad, W. Gao, E. Wu, Z. A. Davies, H. Y. Y. Nyein, S. Challa, S. P. Ryan, H. M. Fahad, K. Chen, Z. Shahpar, S. Talebi, C. Milla, A. Javey, R. W. Davis, *Proc. Natl. Acad. Sci. USA* **2017**, *114*, 4625.
[12] H. Lee, C. Song, Y. S. Hong, M. S. Kim, H. R. Cho, T. Kang, K. Shin, S. H. Choi, T. Hyeon, D. H. Kim, *Sci. Adv.* **2017**, *3*, e1601314.
[13] L. E. Gibson, R. E. Cooke, *Pediatrics* **1959**, *23*, 545.
[14] M. P., M. H. McAloon, *Alcohol.: Clin. Exp. Res.* **1980**, *4*, 391.
[15] A. Huake, P. Simmers, Y. R. Ojha, B. D. Cameron, R. Ballweg, T. Zhang, N. Twine, M. Brothers, E. Gomez, J. Heikenfeld, *Lab Chip* **2018**, *18*, 3750.
[16] G. Cizza, A. H. Marques, F. Eskandari, I. C. Christie, S. Torvik, M. N. Silverman, T. M. Philips, E. M. Sternberg, *Biol. Psychiatry* **2008**, *64*, 907.
[17] Y. J. Hong, H. Lee, J. Kim, M. Lee, H. J. Choi, T. Hyeon, D. H. Kim, *Adv. Funct. Mater.* **2018**, *28*, 1805754.
[18] A. J. Bandodkar, P. Gutruf, J. Choi, K. Lee, Y. Sekine, J. T. Reeder, W. J. Jeang, A. J. Aranyosi, S. P. Lee, J. B. Model, R. Ghaffari, C. J. Su, J. P. Leshock, T. Ray, A. Verrillo, K. Thomas, V. Krishanamurthi, S. Han, J. Kim, S. Krishnan, T. Hang, J. A. Rogers, *Sci. Adv.* **2019**, *5*, eaav3294.
[19] H. Y. Y. Nyein, L. C. Tai, Q. P. Ngo, M. Chao, G. B. Zhang, W. Gao, M. Bariya, J. Bullock, H. Kim, H. M. Fahad, A. Javey, *ACS Sens.* **2018**, *3*, 944.
[20] H. Y. Y. Nyein, M. Bariya, L. Kivimaki, S. Uusitalo, T. S. Liaw, E. Jansson, C. H. Ahn, J. A. Hangasky, J. Q. Zhao, Y. J. Lin, T. Happonen, M. H. Chao, C. Liedert, Y. B. Zhao, L. Tai, J. Hiltunen, A. Javey, *Sci. Adv.* **2019**, *5*, eaaw9906.
[21] J. Moyer, D. Wilson, I. Finkelshtein, B. Wong, R. Potts, *Diabetes Technol. Ther.* **2012**, *14*, 398.
[22] E. V. Karpova, E. V. Shcherbacheva, A. A. Galushin, D. V. Vokhmynina, E. E. Karyakina, A. A. Karyakin, *Anal. Chem.* **2019**, *91*, 3778.
[23] W. Gao, S. Emaminejad, H. Y. Y. Nyein, S. Challa, K. Chen, A. Peck, H. M. Fahad, H. Ota, H. Shiraki, D. Kiriya, D. Lien, G. A. Brooks, R. W. Davis, A. Javey, *Nature* **2016**, *529*, 509.
[24] Y. R. Yang, Y. Song, X. J. Bo, J. H. Min, O. S. Pak, L. L. Zhu, M. Q. Wang, J. B. Tu, A. Kogan, H. X. Zhang, T. K. Hsiai, Z. P. Li, W. Gao, *Nat. Biotechnol.* **2020**, *38*, 217.
[25] J. Choi, R. Ghaffari, L. B. Baker, J. A. Rogers, *Sci. Adv.* **2018**, *4*, eaar3921.
[26] W. Gao, H. Ota, D. Kiriya, K. Takei, A. Javey, *Acc. Chem. Res.* **2019**, *52*, 523.
[27] M. Bariya, L. Li, R. Ghattamaneni, C. H. Ahn, H. Y. Y. Nyein, L. Tai, A. Javey, *Sci. Adv.* **2020**, *6*, eabb8308.
[28] J. Heikenfeld, *Nature* **2016**, *529*, 475.
[29] S. Nakata, M. Shiomi, Y. Fujita, T. Arie, S. Akita, K. Takei, *Nat. Electron.* **2018**, *1*, 596.
[30] L. Tai, T. S. Liaw, Y. Lin, H. Y. Y. Nyein, M. Bariya, W. B. Ji, M. Hettick, C. S. Zhao, J. Q. Zhao, L. Hou, Z. Yuan, Z. Y. Fan, A. Javey, *Nano Lett.* **2019**, *19*, 6346.
[31] J. Q. Zhao, Y. J. Lin, J. B. Wu, H. Y. Y. Nyein, M. Bariya, L. Tai, M. H. Chao, W. B. Ji, G. Zhang, Z. Y. Fan, A. Javey, *ACS Sens.* **2019**, *4*, 1925.
[32] Z. Yuan, L. Hou, M. Bariya, H. Y. Y. Nyein, L. Tai, W. B. Ji, L. Li, A. Javey, *Lab Chip* **2019**, *19*, 3179.
[33] L. Hou, H. Zhao, S. Y. Bi, L. Zhu, Y. M. Xu, Y. X. Lu, *Appl. Surf. Sci.* **2019**, *465*, 320.
[34] Z. H. Ai, L. Z. Zhang, S. C. Lee, W. K. Ho, *J. Phys. Chem. C* **2009**, *113*, 20896.
[35] Y. Lu, J. L. Xu, S. Ren, Y. N. Zhong, X. Gao, S. D. Wang, *RSC Adv.* **2018**, *8*, 20182.
[36] M. Yin, C. Wu, Y. B. Lou, C. Burda, J. T. Koberstein, Y. M. Zhu, S. O'Brien, *J. Am. Chem. Soc.* **2005**, *127*, 9506.
[37] W. S. Kong, M. H. Xiang, L. Xia, M. Y. Zhang, R. M. Kong, F. L. Qu, *Biosens. Bioelectron.* **2020**, *167*, 112481.
[38] C. Q. Dong, H. Zhong, T. Y. Kou, J. Frenzel, G. Eggeler, Z. H. Zhang, *ACS Appl. Mater. Interfaces* **2015**, *7*, 20215.
[39] Z. F. Zhai, B. Leng, N. J. Yang, B. Yang, L. S. Liu, N. Huang, X. Jiang, *Small* **2019**, 1901527.
[40] D. J. Lee, T. H. Cui, *Biosens. Bioelectron.* **2010**, *25*, 2259.
[41] M. Nacef, M. L. Chelaghmia, A. M. Affoune, M. Pontie, *Electroanalysis* **2019**, *31*, 113.
[42] Y. C. Zhang, L. Su, D. Manuzzi, H. V. Monteros, W. Z. Jia, D. Q. Huo, C. J. Hou, Y. Lei, *Biosens. Bioelectron.* **2012**, *31*, 426.
[43] X. S. Du, G. S. Herman, *Sens. Actuators, B* **2018**, *268*, 123.
[44] W. N. Xu, S. G. Dai, X. Wang, X. M. He, M. J. Wang, Y. Xi, C. G. Hu, *J. Mater. Chem. B* **2015**, *3*, 5777.
[45] R. Khan, R. Ahmad, P. Rai, L. Jang, J. Yun, Y. Yu, Y. Hahn, I. Lee, *Sens. Actuators, B* **2014**, *203*, 471.
[46] T. X. Zhu, Y. F. Zhang, L. Q. Luo, X. L. Zhao, *ACS Appl. Mater. Interfaces* **2019**, *11*, 10856.
[47] L. C. Jiang, W. D. Zhang, *Biosens. Bioelectron.* **2010**, *25*, 1402.